METALS AND MATERIALS International, Vol. 11, No. 2 (2005), pp. 121~129

Mechanical Strength Test Method for Solder Ball Joint in BGA Package

Jong-Woong Kim[1], Dae-Gon Kim[1] and Seung-Boo Jung[2,*]

[1] Department of Advanced Materials Engineering, Sungkyunkwan University
300 Cheoncheon-dong, Jangan-gu, Suwon 440-746, Korea
[2] Micro Electronic Packaging Consortium, Sungkyunkwan University
Suwon 440-746, Korea

Ball shear tests were investigated in terms of effects of test parameters, i.e. shear height and shear speed, with an experimental and non-linear finite element analysis in order to evaluate the solder joint integrity of area array packages. The substrate was a common SMD type with solder bond pad openings of 460 μm in diameter. Microstructural investigations were carried out using SEM, and the IMCs were identified with EDS. It was observed that increasing shear height, at fixed shear speed, results in decreasing shear force, while the shear force increased with increasing shear speed at fixed shear height. Excessive shear height could cause some detrimental effects on the test results such as unexpected high standard deviation values or shear tip sliding from the solder ball surface. Low shear height conditions are favorable for screening the type of brittle interfacial fractures or degraded layers in the interfaces.

Keywords: shear height, shear speed, finite element analysis, solder, shear test

1. INTRODUCTION

With the continual miniaturization of electronic components and their increasing functionality, the electronics industry is rapidly switching towards fine pitch devices. Area array components have evolved as a viable solution to meet the requirements of these devices. As packaging density is increasing, solder joint reliability has become a critical issue in the electronic packaging industry [1,2]. A large body of research has recently been conducted in relation to the reliability issues and properties of fine solder joints [3-5]. However, most studies have primarily concentrated on discussions of the mechanical properties or the interfacial reactions between solder and metallization of the substrate. Although a pertinent test method should be used to evaluate certain properties of solder joints in order to improve the reliability of the packages, there has been relatively little research on the test methods or failure mechanisms of the joints [6-8].

Currently, the most popular method to evaluate the strength of a solder ball attachment is the ball shear test. Although this test is simple and convenient to implement, the details of performing the test have not yet been standardized. The JEDEC (Joint Electronic Devices Engineering Council) BGA ball shear standard (JESD22-B117), published in July 2000, prescribed that the gap between the edge of the shear ram and the surface of the substrate should be larger than 0.05 mm and smaller than 25 % of the ball height [9]. Since these specifications are published in terms of a generic procedure based on the case of a common 1.27 mm pitch BGA package, they cannot be applied with a finer pitch or smaller solder ball attachment. In addition, another important ball shear test parameter, shear speed, is not established in the standard. From our previous studies, it was clarified that the shear speed strongly affects the shear force values in the shear test of a solder ball attachment [6,7]. The lack of specification in the shear speed may cause confusion in comparisons of solder ball shear strengths characterized with different displacement rates.

A significant addition to the JESD22-B117 is the incorporation of the ball shear failure mode into the acceptance criteria. The primary impetus for including the failure mode is to provide a means for screening the type of brittle interfacial fractures caused by excessive thick intermetallic compound (IMC) layers [9]. During soldering, the solder alloy melts and then reacts with the metallization of the substrate to form IMCs at the joining interface. While forming a thin IMC layer, it is desirable to achieve a good metallurgical bond [10]. On the other hand, an excessively thick reaction layer is very sensitive to stress and provides sites of initiation and

*Corresponding author: sbjung@skku.ac.kr

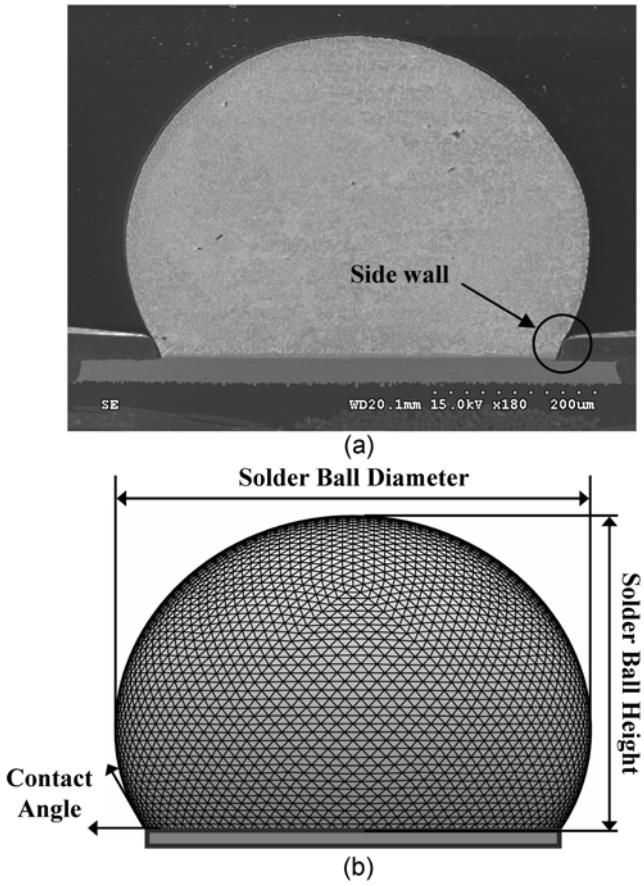

Fig. 1. Geometric profile comparison between actual (a) and predicted solder ball attachment (b).

paths of propagation for cracks, because the layer is brittle and a microstructural mismatch exists between the solder and pad metallization [11]. However, during a BGA ball shear test, the side-walls of SMD (Solder Mask Defined) area array bond pads, as shown in Fig. 1(a), tend to support the solder joint, which can alter the failure mode. Therefore, there is a reluctance to embrace the shear technique for monitoring susceptibility to brittle interfacial failures.

The objectives of this study are to provide an evaluation of the effects of important shear test parameters, such as shear height and shear speed, as well as recommendations for obtaining accurate test results. To provide an example of the shear force change from different shear speed conditions, eutectic Sn-37Pb solder was used in this study. Both an experimental investigation and a non-linear finite element analysis using an elastic-viscoplastic constitutive model were carried out. Two finite element analysis tools, the Surface Evolver developed by Brakke and modified by Chiang and Yuan [12,13] and ANSYS, were used for the analysis. Analytical stress and averaged equivalent plastic strain analyses were performed to interpret the failure mechanisms.

2. EXPERIMENTAL AND ANALYSIS PROCEDURES

2.1. Experimental procedures

The solder composition for the BGA application in this study was eutectic Sn-37Pb. The solder ball had a diameter of 500 μm. The substrate was a SMD type bismaleimide triazine (BT) laminate with subsurface solder bond pads whose nominal size and shape were defined through a circular opening of 460 μm in diameter with 1 mm pitch. The pads were comprised of electroplated Au over Ni over an underlying Cu pad with a thickness of 0.7 and 7.0 μm, respectively. The solder balls were bonded to the BT substrate in a reflow process employing RMA flux with a maximum temperature of 220 °C for 60 s. In order to investigate the shear height effect on the fracture mode of joints having relatively thick IMC layers, an aging condition of 150 °C with 100 h was employed. The microstructures were observed with a scanning electron microscope (SEM) and the compositions of the resulting IMCs were measured by an energy dispersive spectrometer (EDS). Shear tests were conducted using a global bond tester (Dage-4000s, Richardson Electronics Ltd.) under various test conditions. The shear test conditions are given in Tables 1 and 2. The fracture mode of each test site was examined after shear testing to evaluate the mode of failure.

2.2. Finite element analysis

The reflow geometry of the solder ball was predicted using the Surface Evolver program, which is an energy-based method for predicting the shape of a liquid body. To simulate the geometric shape of a liquid body, the Surface Evolver deconstructs the initial simplex surface of the liquid body into a set of triangular facets and then iterates these facets toward a minimal energy equilibrium situation using a gradient descent method. Under the condition of static equilibrium, the total energy of a liquid body is generally comprised of three major energy portions, i.e. surface tension energy, gravitational energy, and external energy related to body volume change [12,13]. Fig. 1 shows a general cross-sectional view of a reflowed Sn-37Pb solder joint and the 3-dimensional (3-D) finite element model predicted by the Surface Evolver. To confirm the accuracy of the geometric prediction, actual measurements of the solder ball were compared

Table 1. Examined shear height conditions

Shear speed (μm/s)	Shear height (μm)					
200	10	30	50	70	90	120

Table 2. Examined shear speed conditions

Shear height (μm)	Shear speed (μm/s)						
50	10	50	100	200	300	400	500

Table 3. Comparison of solder ball shape between actual and predicted model

	Actual model	Predicted model
Solder ball diameter (μm)	537.4	536.7
Solder ball height (μm)	353.6	354.4
Contact angle (degree)	60.19	61.03

to the prediction. The solder ball diameter, solder ball height, and contact angle for the actual and predicted solder ball are compared in Table 3, revealing a close agreement between the Surface Evolver prediction and the measured values.

The key points of the solder ball surface were obtained from the Surface Evolver prediction using a curve fitting program, and then used to construct the solder ball model in ANSYS software. For analysis time saving, 2-D elastic-viscoplastic finite element simulation methodologies were utilized to predict the effects of the ball shear parameters on shear force. The components of the finite element simulation included a reflowed solder ball, a BT substrate, a subsurface Cu pad, and an electroplated Ni layer. The shear ram was considered as a rigid body. The surface-to-surface target element (TARGE169) and the contact element (CONTA172) were employed to simulate the contact between the shear ram and the solder ball. Figs. 2(a) and (b) show the overall 2-D finite element model for the ball shear test and a magnified view near the left side of the Ni layer, respectively.

Since the test temperature was in excess of a homologous temperature of 0.5, linear, non-linear, time dependent, and independent material properties were incorporated in the finite element model [14-17]. In the present work, the Anand model was employed to represent the viscoplastic behavior of solder. The Anand model is a unified framework for viscoplastic behavior of solder materials, in which plasticity and creep are unified and described by the same set of flow and evolutionary equations. However, the Anand model is only available for VISCO10X elements in ANSYS, and thus convergence is difficult and time consuming. Therefore, some modifications were evolved to extract only the steady state creep behavior from the Anand model. Details of the modifications can be found in our previous paper [6].

The Anand model is simplified to the hyperbolic sine creep form, resulting in the following steady state creep equation.

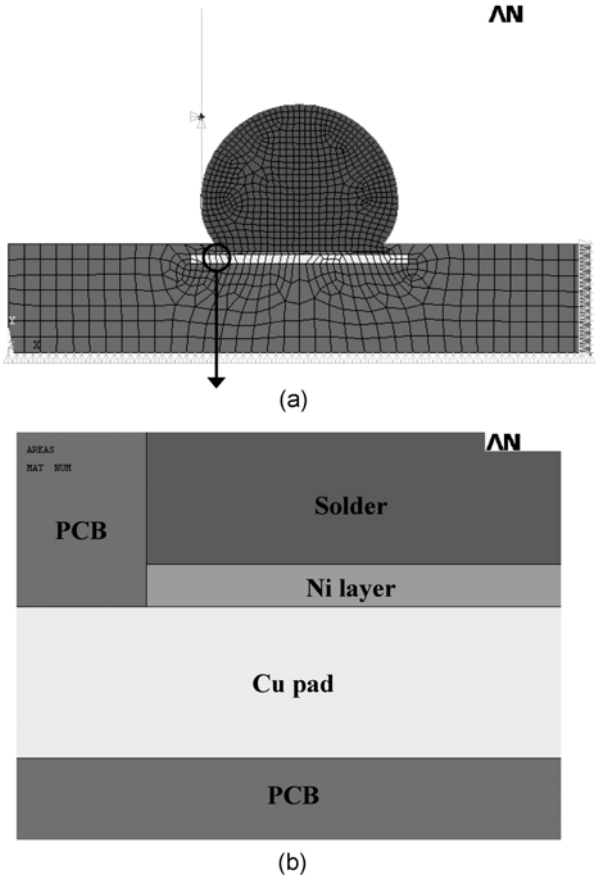

Fig. 2. Finite element model for the ball shear test (a) and magnified view near the Ni layer (b).

$$\frac{d\varepsilon_p}{dt} = A\exp\left(-\frac{Q}{RT}\right)[\sinh(\alpha\sigma)]^{1/m} \quad (1)$$

where $d\varepsilon_p/dt$ is the steady state creep strain rate, A is the pre-exponential factor, Q is the activation energy, R is the gas constant, T is the absolute temperature, α is the stress level at which the power law dependence breaks down, σ is the applied stress, and m is the strain rate sensitivity of stress. It should be noted that Eq. 1 is exactly the same form of input for the implicit creep model (TBOPT=8) of ANSYS, release 6.1. This creep option was combined with Multilinear Isotropic (MISO) hardening using von Mises plasticity to represent the viscoplastic properties of the solder material. The linear elastic material properties and steady state creep constants are

Table 4. Linear elastic material properties for BGA assemblies

Material	Young's Modulus (MPa)	Poisson's Ratio	Density (g/cm^3)
Sn-37Pb	29,800	0.40	8.4
Cu	117,000	0.34	8.9
Ni	213,000	0.31	8.9
BT Substrate	14,000	0.39	1.2

Table 5. Input parameters for creep analysis

	A (1/sec)	α (1/KPa)	m	*Q/R* (K)
Sn-37Pb	1.09E7	8.7E-5	0.316	9,400

given in Tables 4 and 5, respectively. The steady state creep constants were converted from the Anand model constants.

3. RESULTS AND DISCUSSION

An average incremental equivalent plastic strain analysis was performed to determine the failure mode of the solder ball under the shear test, because the load on the pad site of the solder ball during a shear test is a mixture of tensile, shear, and compressive forces, especially at the corners of the solder [18]. Fig. 3(a) plots the distribution of the averaged equivalent plastic strain for the base case. From Fig. 3(a), the high plastic strain region in the solder ball is found to be near the contact point between the shear ram and the solder, and has subsequently expanded through the solder parallel to the substrate. This implies a strong likelihood of crack initiation and growth through this region. A cross-sectional view of the solder ball after the shear test is shown in Fig. 3(b). Comparing Figs. 3(a) and (b), the shear failure mode of solder ball joint determined by computational analysis shows good correlation with the actual solder ball failure mode under the shear test. Nearly all test specimens exhibited this ductile mode of failure, which is caused by the softness of the Sn-37Pb solder.

Fig. 4 shows the force-displacement curves from the experiment and modeling computation at the base condition. The graphs from the experiment and modeling show similar concave down behavior except for the first stage of the curves where a concave up region is displayed. This is likely due largely to experimental errors such as flux residues. Alternately, the reflowed ball shape may produce a concave up Hertzian loading curve characteristic of increased contact area with the ram of the shear tester. From the two results noted above, it could be concluded that the finite element analysis used in this study is sufficiently reliable.

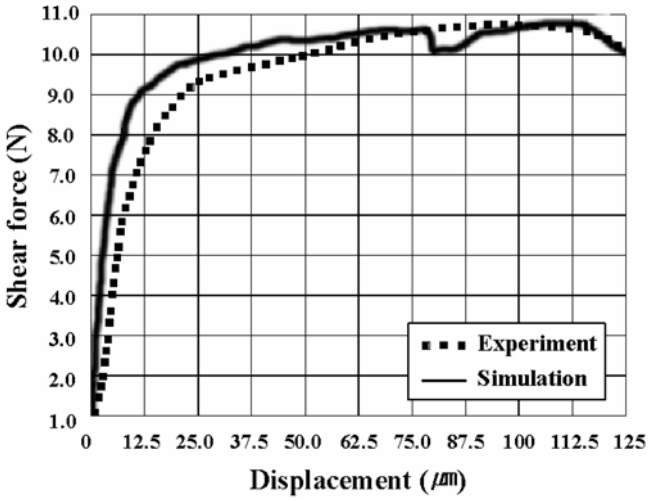

Fig. 4. Force-displacement curve in the base case conditions (shear height: 50 μm, shear speed: 200 μm/s).

Figs. 5(a) and (b) show back scattered electron (BSE) micrographs of the interface between the Sn-37Pb solder and the Au/Ni electroplated layer on the Cu pad, corresponding to as-reflowed condition and aged condition at 150 °C for 100 h, respectively. The light and dark regions in the micrographs are α_{Pb} domains and β_{Sn} matrix, respectively. A lamellar structure of α_{Pb} and β_{Sn} was formed [19]. This microstructure could be considered an influential factor controlling the mechanical properties of the solder, which corresponds with

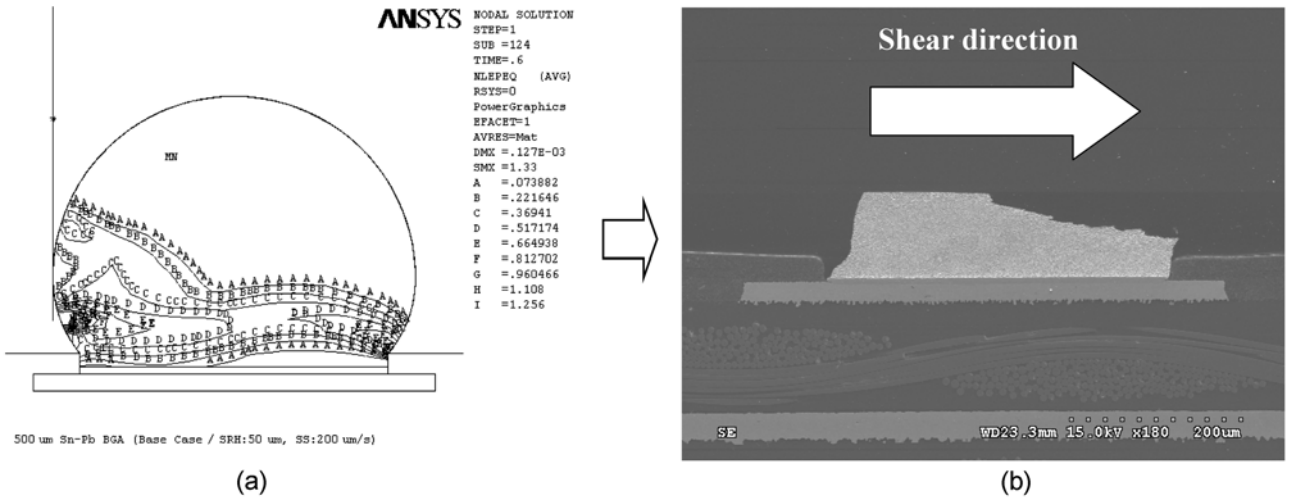

Fig. 3. Contour plot of an averaged equivalent plastic strain analysis (a) and the cross-sectional view after the ball shear test (b) in the base case conditions (shear height: 50 μm, shear speed: 200 μm/s).

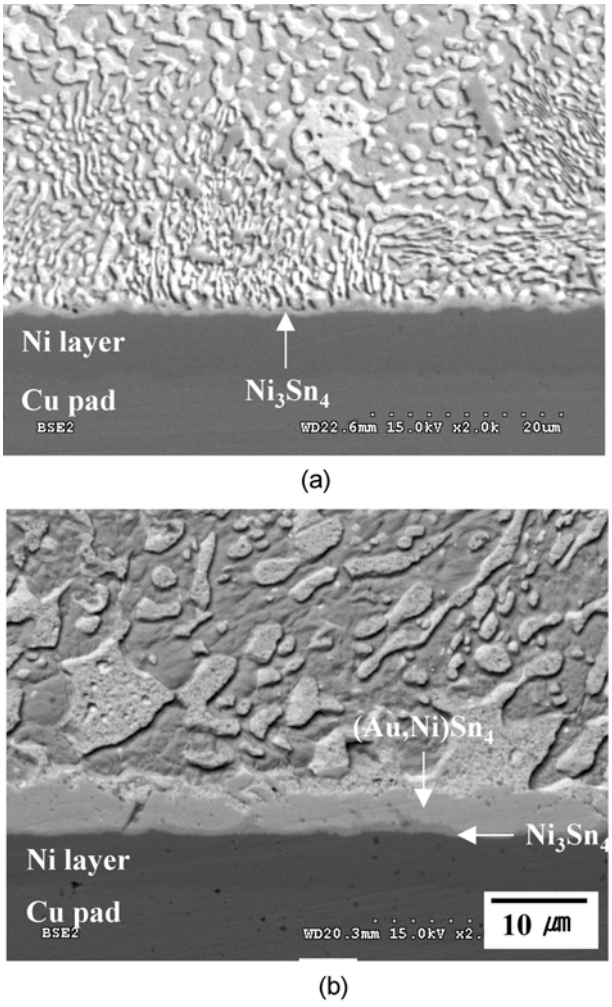

Fig. 5. SEM micrographs of Sn-37Pb solder joint interfaces: (a) as-reflowed condition and (b) aged at 150 °C for 100 h condition.

the Anand constitutive model and the MISO hardening model. At the as-reflowed interface between the solder and substrate, a layer of Ni_3Sn_4 IMC having a thickness of approximately 0.8 μm was formed, while the Au layer appears to have dissolved or reacted with the solder, leaving no observable Au at the interface. However, after aging at 150 °C for 100 h, a layer of $AuSn_4$ containing a certain amount of Ni dissolved, i.e. $(Au,Ni)Sn_4$, was observed above the Ni_3Sn_4 layer. In Fig. 5(b), the upper bright thick layer is $(Au,Ni)Sn_4$, while the lower dark thin layer was analyzed to be Ni_3Sn_4 IMC. This is consistent with the results in the literature for the reaction between Sn-37Pb and Au/Ni plated Cu [20,21]. An excessively thick IMC layer is sensitive to stress and provides sites of initiation and paths of propagation for cracks because the layer is brittle and a microstructural mismatch exists between solder and metallization. Therefore, growth of the IMC layer could degrade the solder ball shear strength. For this reason, in term of electronic

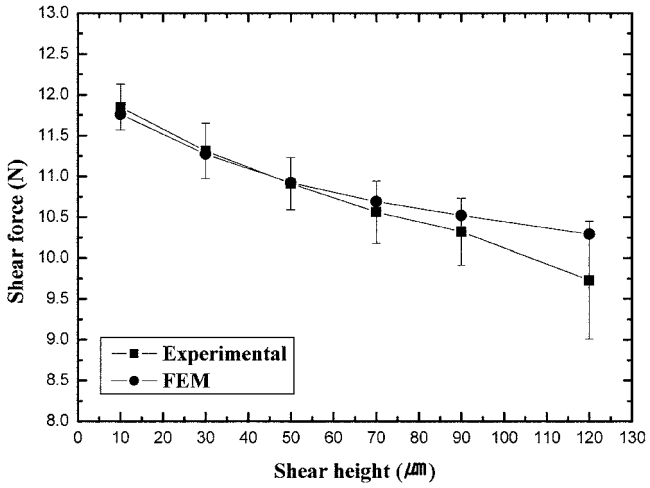

Fig. 6. Shear force variations with increasing shear height (shear speed: 200 μm/s).

package reliability, it is important to screen the brittle interfacial fracture or to identify weak interfaces in solder joints when high temperature storage, burn-in, or extended bake-out creates thick IMC layers.

Fig. 6 shows the shear force variations from both experiment and computational modeling under increasing shear height. Experimentally, for each test condition, 30 solder balls were sheared to failure. The shear force decreased with increasing shear height and reached the minimum value at the highest height. This indicates that the resistance to plastic deformation is increased by increasing the contact area between the shear ram and bulk solder. In the same manner, the computational results indicate that the shear force decreased with increasing shear height. The phenomenological situation and the mathematical calculations are in qualitative agreement, supporting the logic that the decrease in shear force with increasing shear height is a direct consequence of the geometrical shape of the solder ball. However, it should also be noted that, in the cases of over 70 μm shear height, both mismatches between the experimental and computational results and standard deviation values from the experimental results were increased. These discrepancies are attributed to the extremely confined contact area between the shear ram and solder and the severe local deformation in the solder (the edge of the shear ram cuts deep into the solder ball due to the high ram height). Therefore, for the high shear probe height, the shear force results from the experiment could be more susceptible to experimental factors such as application of an indefinite quantity of solder to the pad resulting in different ball shape, flux residues on the ball surface, compliance of the shear test fixture, oxidation at the BGA surface, etc. From an engineering point of view, excessive shear height should be removed from the test conditions.

Fig. 7 illustrates the distributions of the average equivalent plastic strain after the simulation of shear test under different

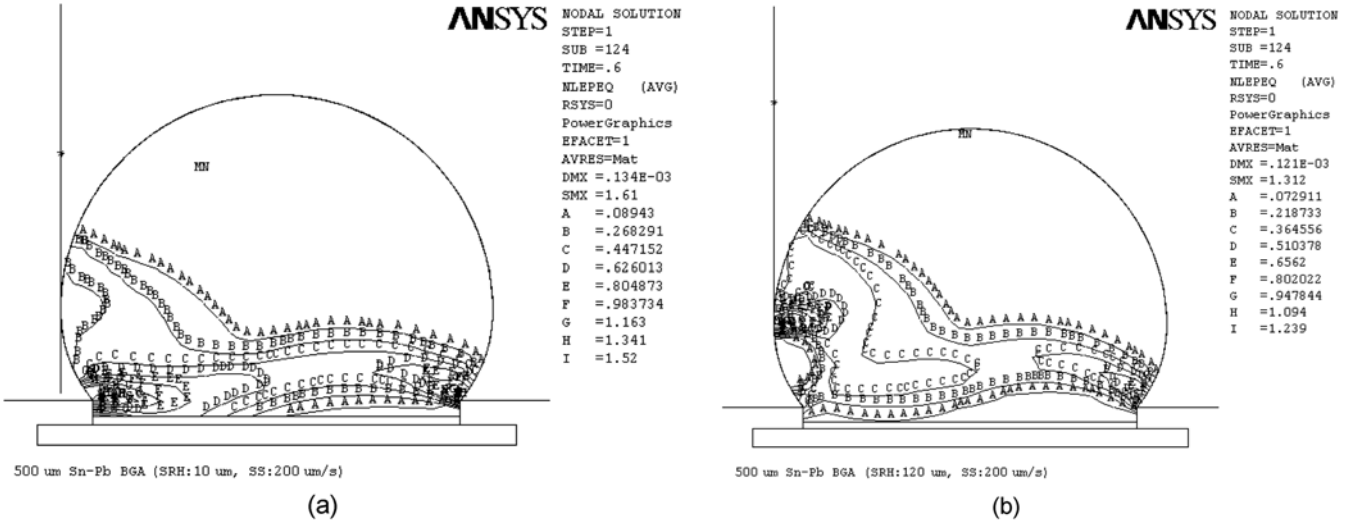

Fig. 7. Distributions of averaged equivalent plastic strain after shear test simulation of Sn-37Pb solder joints: (a) shear height of 10 μm and (b) shear height of 120 μm.

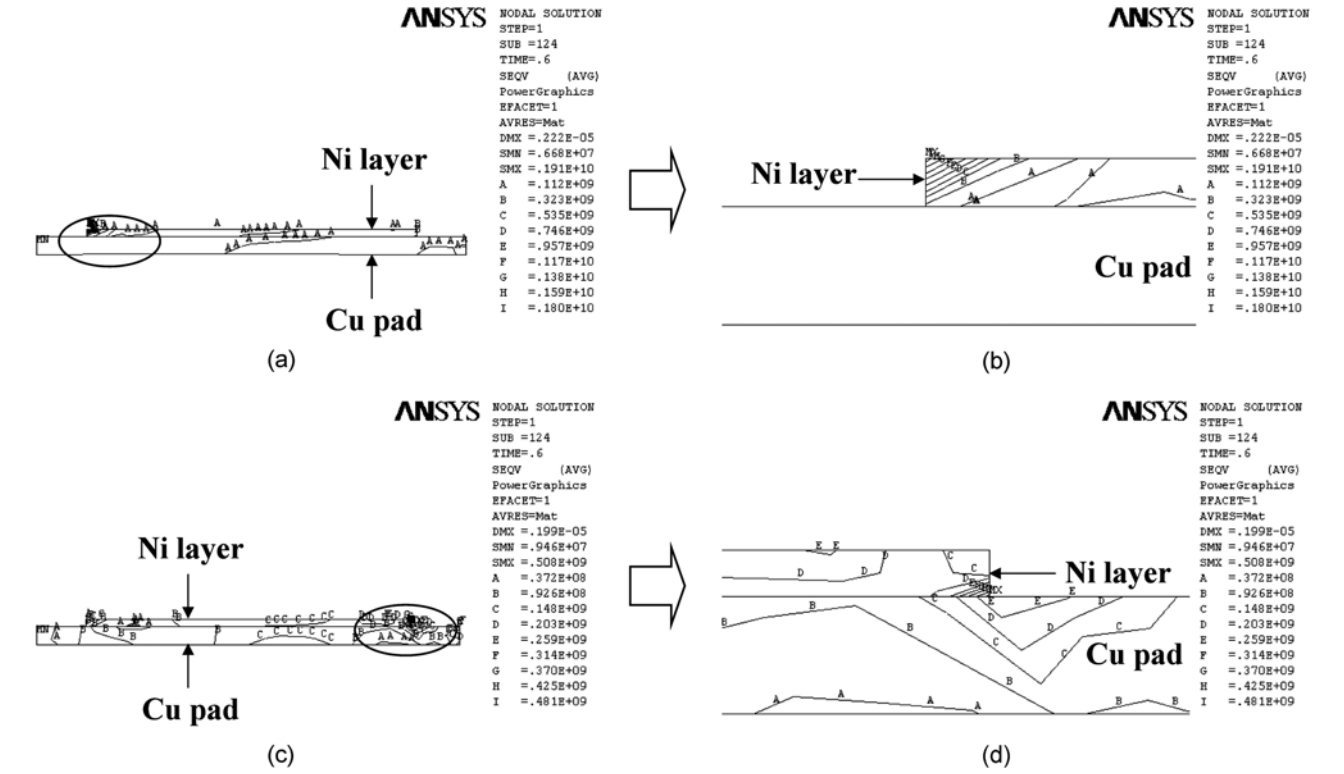

Fig. 8. Von Mises stress contours within the Cu pad and Ni layer: (a) and (b) shear height of 10 μm, (c) and (d) shear height of 120 μm.

shear height conditions. As shown here, the strain has densely accumulated in the right above the Ni layer for the case of 10 μm shear height, while it is spread out in the upper region of the solder for the case of 120 μm shear height. Furthermore, the maximum value of strain in Fig. 7(a) is higher than that of Fig. 7(b). Therefore, it could be deduced that, if the IMC layer between the solder and pad metallization is sufficiently thick, brittle interfacial failure could occur more easily in the cases of lower shear height.

Fig. 8 presents the von Mises stress contours within the Cu pad and Ni layer. The figures indicate that the application of shear loads to a multi-phase structure results in the formation of a singularity phenomenon, i.e. a stress concentration, at the corner of the common boundary of two different materials [11]. This is due to the phase discontinuity that occurs at this boundary. However, the location of the maximum stress

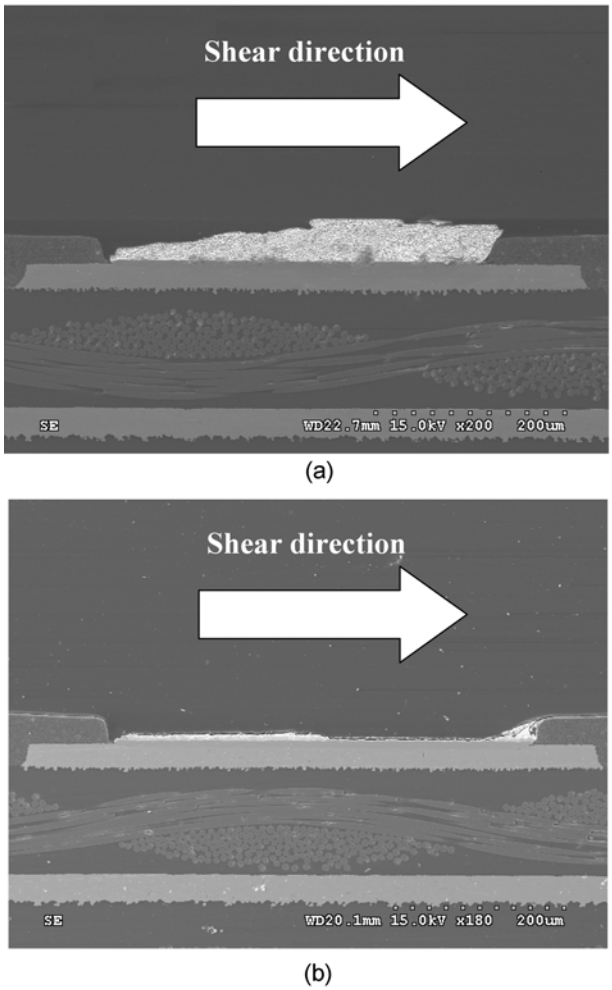

Fig. 9. Cross-sectional views after shear test at 10 μm shear height: (a) as-reflowed condition and (b) aged at 150 °C for 100 h condition.

varies between the two cases, i.e., for shear heights of 10 and 120 μm. The maximum stress region is located in the left corner of the Ni layer when the shear height is 10 μm, while the stress is concentrated in the right corner of the Ni layer, which could not initiate a failure path when the shear height is 120 μm. This indicates that the cases with lower shear height could screen brittle interfacial fractures or degraded layers in the interfaces more easily. Although the maximum stress occurs within the Ni layer, cracking does not readily occur near this layer because the strengths of the IMCs or Ni layer are occasionally greater than those of solders. Accordingly, when the thickness of the interfacial IMC layer is thicker, brittle interfacial failure could occur for the cases of lower shear height.

Figs. 9(a) and (b) show the typical fractured cross-sectional views of the as-reflowed and aged specimens, respectively, under the conditions of 10 μm shear height with 200 μm/s shear speed. As shown in the figures, the failure type was converted from a ductile fracture mode to a brittle

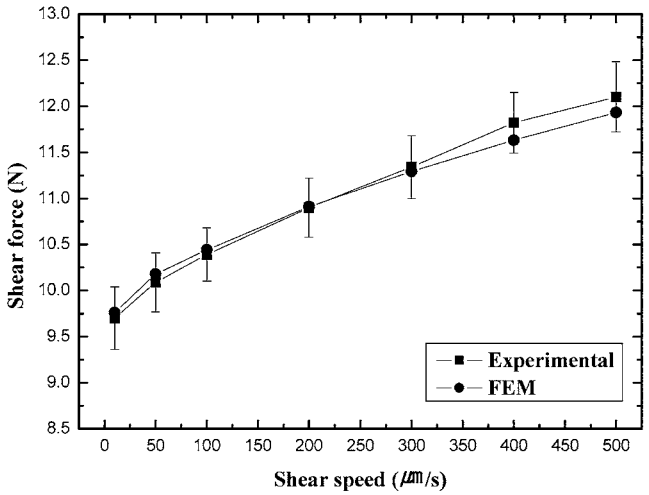

Fig. 10. Shear force variations with increasing shear speed (shear height: 50 μm).

interfacial fracture mode. In the same conditions of Fig. 9(b), about 65 % of the specimens exhibited this mixed mode of brittle and ductile fracture, while the remaining specimens showed the brittle interfacial fracture mode. This correlates well with the simulation results described above.

The shear force variations of experiment and computational modeling under increasing shear speed are shown in Fig. 10. The shear force is proportional to the shear speed and reaches a maximum value at the highest shear speed in both the experimental and computational results. This indicates that the increase in shear force with increasing shear speed is a direct consequence of the material properties including both time-independent plastic hardening and time-dependent creep. According to Nadai's mathematical analysis, a general relationship between flow stress and strain rate, at constant strain and temperature, can be expressed by [22,23]

$$\sigma = C\left(\frac{d\varepsilon}{dt}\right)^{s}\Bigg|_{\varepsilon,T} \tag{2}$$

where s is known as the strain-rate sensitivity and C is a constant. The exponent s can be obtained from the slope of a plot of $\log\sigma$ vs. $\log(d\varepsilon/dt)$. In ordinary metals having a high melting point, the strain-rate sensitivity (s) is quite low (≤ 0.1) at room temperature, but s increases with temperature, especially at temperatures above a homologous temperature of 0.5. Because room temperature is higher than half of the melting point of solder in absolute temperature, the strain rate or displacement rate is very important with respect to the stress flow properties. According to our previous studies, the shear force of low melting point In-48Sn solder increased from about 1.6 to 3.0 N with a shear speed ranging from 10 to 700 μm/s, i.e. an approximately 88 % rise in the shear force. This is well explained by the theory noted above [7].

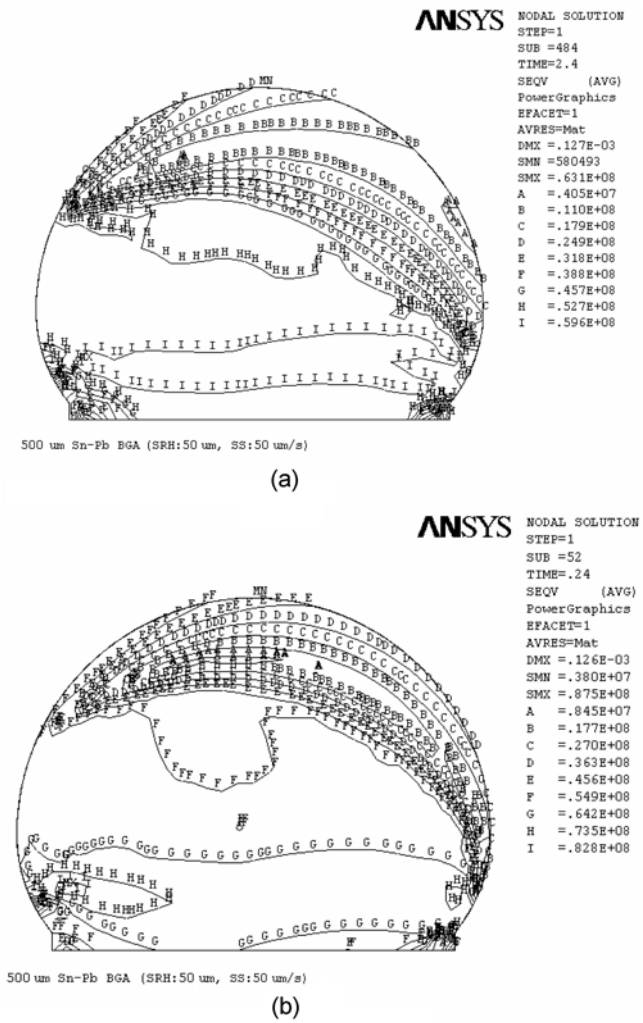

Fig. 11. Von Mises stress contours within the solder: (a) shear speed of 50 μm/s and (b) shear speed of 500 μm/s.

Fig. 11 shows the von Mises stress contour analyses of Sn-37Pb for the two test conditions, i.e., shear speed of 50 and 500 μm/s with a fixed shear height of 50 μm. The highest stress region of the only solder ball covered the fracture locations, which are shown in Fig. 3(b). This indicates that the ball shear mode is also closely related to the high region of von Mises stress contours. In the figure, the von Mises stress values increase with increasing shear speed, giving rise to increasing ball shear forces, as indicated in Fig. 10.

4. CONCLUSIONS

Analyses of a test method for the strength of eutectic Sn-37Pb BGA solder joints were conducted. From the results the following conclusions are drawn.

1. The reflowed solder ball shape was successfully predicted by the energy-based simulation tool, i.e. Surface Evolver. The results from the simulation using ANSYS, such as the averaged equivalent plastic strain and the force-displacement curves, indicated that the finite element analysis used in this study was reasonably reliable.

2. In the as-reflowed condition, only an Ni_3Sn_4 IMC layer was formed at the interface between the Au/Ni layer on the Cu pad and Sn-37Pb solder, having a thickness of about 0.8 μm. However, after aging at 150 °C for 100 h, a continuous $(Au,Ni)Sn_4$ IMC layer was additionally observed at the interface. The thickness of the $(Au,Ni)Sn_4$ layer was about 6 μm. The microstructure of solder alone showed a lamellar structure consisting of α_{Pb} and β_{Sn}.

3. Increasing shear height, at fixed shear speed, had the effect of decreasing shear force in both the experimental and computational results. The decreases in shear force were attributed to the decreased contact area between the shear ram and bulk solder.

4. Overly high shear height could have negative effects on the test results, e.g. unexpected high standard deviation values or shear tip sliding from the solder ball surface. Therefore, a shear height exceeding 20 % of the solder ball height should be avoided.

5. From the computational results, the relatively low shear height conditions were found to be favorable for screening the type of brittle interfacial fractures or degraded layers in the interfaces. This correlated well with the experimental results performed with aged samples.

6. The shear force increased with increasing shear speed at a fixed shear height of 50 μm. The tendency of the results corresponds well with those of other studies.

The results obtained from this study should be very helpful for the electronics industry to determine the acceptance criteria for products or interpret their testing data. However, broader investigations into shear test of finer pitched packages using various lead-free solders are essential.

ACKNOWLEDGMENTS

This was supported by grant No. R01-2004-000-10572 from the Basic Research Program of the Korea Science & Engineering Foundation.

REFERENCES

1. S. Ho, G. Wang, M. Ding, J. Zhao, and X. Dai, *Microelectronics Reliability* **44**, 719 (2004).
2. P. Towashiraporn, K. Gall, G. Subbarayan, B. McIlvanie, B. C. Hunter, D. Love, and B. Sullivan, *Int. J. Fatigue* **26**, 497 (2004).
3. L. C. Shiau, C. E. Ho, and C. R. Kao, *Soldering and Surface Mount Technology* **14**, 25 (2002).
4. S. K. Kang, W. K. Choi, M. J. Yim, and D. Y. Shih, *J. Electron. Mater.* **31**, 1292 (2002).
5. J. W. Yoon, S. W. Kim, and S. B. Jung, *Mater. Trans.* **45**,

727 (2004).
6. J. W. Kim and S. B. Jung, *Mater. Sci. Eng. A* **371**, 267 (2004).
7. J. W. Kim, D. G. Kim, J. M. Koo, and S. B. Jung, *Proceedings of 5th International Conference on Electronics Materials and Packaging* (ed., Sung Yi), p. 282, IEEE, Singapore (2003).
8. S. W. Ricky Lee and X. Huang, *Soldering and Surface Mount Technology* **14**, 45 (2002).
9. JESD22-B117, *JEDEC Solid State Technology Association* (2002).
10. J. W. Yoon, C. B. Lee, D. U. Kim, and S. B. Jung, *Met. Mater. -Int.* **32**, 1195 (2003).
11. H. T. Lee, M. H. Chen, H. M. Jao, and T. L. Liao, *Mater. Sci. Eng. A* **358**, 134 (2003).
12. X. Zhao, C. Wang, G. Wang, G. Zheng, and S. Yang, *IEEE Transactions on Electronics Packaging Manufacturing* **23**, 87 (2000).
13. K. N. Chiang and C. A. Yuan, *IEEE Transactions on Advanced Packaging* **24**, 158 (2001).
14. M. Amagai, *Microelectronics Reliability* **39**, 1365 (1999).
15. J. K. Lin, A. D. Silva, D. Frear, Y. Guo, S. Hayes, J. W. Jang, L. Li, D. Mitchell, B. Yeung, and C. Zhang, *IEEE Transactions on Electronics Packaging Manufacturing* **25**, 300 (2002).
16. J. H. Lau and S. W. Ricky Lee, *IEEE Transactions on Electronics Packaging Manufacturing* **25**, 51 (2002).
17. J. H. Lau and Y. H. Pao, *Solder Joint Reliability of BGA, CSP, Flip Chip, and Fine Pitch SMT Assemblies*, p. 91, McGraw-Hill, Inc., NY (1997).
18. K. C. Chang and K. N. Chiang, *IEEE Transactions on Components and Packaging Technologies* **27**, 373 (2004).
19. M. A. Matin, W. P. Vellinga, and M. G. D. Geers, *Acta mater.* **52**, 3475 (2004).
20. C. E. Ho, R. Zheng, G. L. Luo, A. H. Lin, and C. R. Kao, *J. Electron. Mater.* **29**, 1175 (2000).
21. J. W. Choi, H. S. Cha, and T. S. Oh, *Met. Mater. -Int.* **9**, 273 (2003).
22. G. E. Dieter, *Mechanical Metallurgy*, p. 139, McGraw-Hill, Inc., NY (1988).
23. A. Nadai, *Theory of Flow and Fracture of Solids*, p. 535, McGraw-Hill, Inc., NY (1950).